Journal of Non-Crystalline Solids 357 (2011) 3830–3840

Contents lists available at SciVerse ScienceDirect

Journal of Non-Crystalline Solids

journal homepage: www.elsevier.com/ locate/ jnoncrysol

Development of CaZn based glassy alloys as potential biodegradable bone graft substitute

W. Jiao [a], H.F. Li [b], K. Zhao [a], H.Y. Bai [a], Y.B. Wang [b], Y.F. Zheng [b,*], W.H. Wang [a,*]

[a] Institute of Physics, Chinese Academy of Sciences, Beijing 100190, China
[b] Department of Advanced Materials and Nanotechnology, College of Engineering, Peking University, Beijing 100871, China

ARTICLE INFO

Article history:
Received 10 June 2011
Received in revised form 31 July 2011
Available online 24 August 2011

Keywords:
Biodegradable metal;
Mechanical properties;
Corrosion;
Cytocompatibility;
Bone graft substitutes

ABSTRACT

We report the development of a CaZn based bulk glassy alloy (BGA) with combining properties of low Young's modulus, high fracture strength, good corrosion resistance and cytocompatibility, which make it be potential as biodegradable bone graft substitute. Compared to commonly investigated biodegradable metals, the Young's modulus of the BGA is closer to that of cortical bone, and its fracture strength reaches 600 MPa, which is 2 times higher than that of pure magnesium. The magnetic susceptibility of the CaZn based BGA is as low as 22.3×10^{-6}, which is compatible with magnetic resonance imaging (MRI) diagnosis. The BGAs also show slow degradation rate and good cytocompatibility. The new class of biodegradable CaZn based BGAs enriches the family of biomaterials, and the work has implications for developing new biodegradable alloys with active elements. The formation and the origins of excellent properties of the BGA are discussed.

1. Introduction

In the latest decade, biodegradable metals as a prominent class of biomedical materials has received great attention because they can be used as coronary stent and bone graft substitute [1–3]. Up to now, magnesium alloys [4–9] and iron alloys [2,10,11] are two dominant classes of metals with the temporary function. The very slow degradation rate and possibly interfering with magnetic resonance imaging (MRI) diagnosis place severe limitation on clinical application of iron alloys [2]. The main shortcoming of Mg alloys for biomedical applications is their high corrosion rate. Recently, it is found that the surface modification, [12–15] such as Ca–P coating, [12] micro-arc oxidation,[13] alkali-heat treatment [14] and biodegradable polymer-based coating,[15] and alloying with appropriate elements can modulate the corrosion rate of Mg [16–18]. The advancement in tailoring degradation rate of Mg alloys and successful clinical application of calcium phosphate biomaterials [9,19,20] inspire us to develop the calcium alloys as potential biodegradable material.

Calcium, which is immediately below magnesium as the same group member in periodic table, is the most abundant mineral in the human body, and is important to human metabolism [21,22]. It is reported that Ca composes approximately 38% of the mineral content of bone, [21] and the content of Ca is about 1000–1500 g in adult human body, and 99% of which is found in the bones in the form of hydroxyapatite, [23] whereas it is estimated that about 25 g Mg was stored in the body. Calcium also plays a positive effect on bone accretion and bone mineral [21]. Moreover, the extracellular ionized Ca is involved in many physiological functions, such as muscle contraction, neuronal activity, cellular permeability, hormone secretion, and enzyme activity [23]. The concentration of Ca in blood is about 2.5 mmol/L, 10 mg/100 mL, higher than that of Mg (0.9 mmol/L) [22,24]. Calcium homeostasis is maintained by hormonal regulation of the intestinal absorption and renal reabsorption. The Ca concentration of the blood and body fluids can be kept from varying erratically by regulating the rates of bone calcium deposition and resorption [24]. Optimal Ca requirement recommended by the National Institutes of Health is about 1000 mg/day for adult [23]. Besides, the density of calcium is 1.55 g/cm^3, which is the lightest alkaline earth metal. And the Young's modulus of calcium is only 20 GPa, which falls in the same range as that of cortical bone [25].

However, calcium is chemically active, the application faces a series of more serious challenges. The main obstacle is high degradation rate, especially in physiologic environment containing chloride ion. The standard potential of calcium is −2.868 V (Ca/Ca^{2+}, vs. SHE), which is more negative than that of Mg [−2.372 V (Mg/Mg^{2+}, vs. SHE)]. If putting Ca and Mg together, Ca would act as anode and corrode firstly. For pure Mg or simple Mg alloy, the degradation rate is still too fast to satisfy the requirement that implant has to perform for at least 12 weeks, [8] and the situation faced by Ca would be more severe. To our present knowledge, none of satisfied Ca alloys was reported. Besides, the yield strength of pure Ca is too small to be used for load-bearing alone. Especially in physiologic environment, the mechanical properties would lose gradually [6].

Bulk glassy alloy (BGA) is a newcomer to the glassy material family. The combining properties of high fracture strength and toughness, high corrosion and wear resistance and low elastic constants comparing

* Corresponding authors. Fax: +86 10 82640223.
E-mail addresses: yfzheng@pku.edu.cn (Y.F. Zheng), whw@iphy.ac.cn (W.H. Wang).

0022-3093/$ – see front matter © 2011 Elsevier B.V. All rights reserved.
doi:10.1016/j.jnoncrysol.2011.08.003

with its crystalline counterpart inspires great attention to use the BGA as biomedical material [26–32]. The formation and properties of the Ca-based BGA have been recently studied [33]. However, the results show that the degradation rate of the previously reported Ca-based BGAs is still too high to satisfy the biodegradable applications [34]. Simple surface modification cannot effectively reduce the corrosion rate because the protective film and BGA substrate would split after immersion in the solution [35]. Considered that alloying element is another effective method to improve corrosion resistance, we try to alloy Zn element in the Ca based BGA because zinc is widely used as anti-corrosion agent and is also an essential element for humans. There is one to two grams zinc in the human body, and it is a cofactor for several enzymes, such as alkaline phosphatase (necessary for bone mineralization) and collagenase (essential for the development of the collagenous structure of bone) [21]. Zinc also plays an important role in osteoblast adhesion and operation [36]. Recently, it is verified that the degradation rates of Mg–Zn alloys can be much slowed down compared to pure Mg, [16,17] and the Mg–Zn glassy alloys shown good biocompatibility. Alloying with rare earth elements is another effective way to improve corrosion resistance and mechanical properties of magnesium [18,37]. The results of biocompatibility show that rare earth elements did not lead to significant changes in metabolic activity over a wide concentration range [38]. Ytterbium has unlimited solubility in calcium and has been found to be effective for improving corrosion resistance, glass-forming ability and mechanical properties of metallic glass. On the other hand, the glassy alloy, frozen liquid configuration, can alloy high content of zinc exceeding its solid solubility at room temperature in Ca according to Ca–Zn phase diagram, [39] and the Ca–Zn alloy with high Zn content can be homogeneous in concentration and structure, which can minimize the galvanic corrosion. In addition, the Young's modulus of glassy alloy is generally lower by 20%–40% than that in its crystalline counterpart, [30,40] while the fracture strength is close to the theoretical strength of the alloy [41].

In this paper, we report the formation and property improvements of a series of CaZn based BGAs. We compared the features and properties of the CaZn based BGA with widely investigated biomedical metals especially Mg alloys, and evaluated the feasibility of the CaZn based BGAs to be used as biodegradable bone graft substitute from the viewpoint of mechanical, physical, corrosion and biocompatibility. We have interpreted the reasons for the good corrosion resistance and cytocompatibility of the CaZn based BGAs.

2. Experimental procedure

2.1. Materials fabrication and characterization

The CaZnMgYb alloys with nominal compositions listed in Table 1 were fabricated by induction melting of Ca, Zn, Mg and Yb (purity better than 99%, 99.99%, 99.9% and 99.95%, respectively) in quartz crucible in a purified argon atmosphere. The alloy melts were injected into copper molds to get 2 mm diameter cylinder or 1 mm thick plate shapes. The phase of the as-cast alloy was identified by X-ray diffraction (XRD) using a MAC M03 diffractometer with Cu $K\alpha$ radiation source. Differential scanning calorimetry (DSC) was performed under a purified argon atmosphere in a Mettler Toledo DSC822e with a heating rate of 20 $K \cdot min^{-1}$. The density ρ was measured by Archimedes' principle in absolute alcohol.

Table 1
Thermal parameters of representative CaZn based BGA.

BGA	T_g (K)	T_x (K)	ΔT_x (K)	T_m (K)	T_l (K)	T_{rg}
$Ca_{65}Zn_{20}Mg_{15}$	370	402	32	617	635	0.583
$Ca_{48}Zn_{30}Mg_{14}Yb_8$	382	432	50	634	653	0.585
$Ca_{32}Zn_{38}Mg_{12}Yb_{18}$	391	439	48	634	727	0.539

2.2. Mechanical and physical properties measurement

Samples for mechanical property measurement were cut from the as-cast 2 mm rods with a gauge aspect ratio of 2:1 according to ASTM standards [42]. Uniaxial compression was performed on an Instron 5500R1186 testing machine at a constant strain rate of $1 \times 10^{-4}\ s^{-1}$ at room temperature. For physical property measurement, 2 mm thick disk samples were cut from cylinder shaped glassy alloys with 2 mm in diameter. Magnetic susceptibility measurement was carried out in superconducting quantum interference device (SQUID) magnetometer at room temperature, the applied magnetic field of which can reach up to 5 T.

2.3. Immersion test

The immersion test was carried out in the Hank's solution [43] (NaCl 8.0 g, $CaCl_2$ 0.14 g, KCl 0.4 g, $NaHCO_3$ 0.35 g, glucose 1.0 g, $MgCl_2 \cdot 6H_2O$ 0.1 g, $Na_2HPO_4 \cdot 2H_2O$ 0.06 g, KH_2PO_4 0.06 g, $MgSO_4 \cdot 7H_2O$ 0.06 $g \cdot l^{-1}$) according to ASTM-G31-72 [44], and the ratio of surface area to solution volume was 1 cm^2:20 ml. The initial pH value was adjusted to 7.4, and the temperature was kept at 37 °C using water bath. The samples were cut from 1 mm thick plate, polished with SiC paper up to 1200 grit and ultrasonically cleaned with absolute alcohol and distilled water sequently prior to immersion. After different immersion periods, the samples were removed from Hank's solution, gently rinsed with absolute alcohol and distilled water sequently, and dried at room temperature. The surface morphologies and chemical composition of the samples were characterized by scanning electron microscope (SEM, Hitachi S-4800), equipped with energy-disperse spectrometer (EDS) attachment, and the corrosion products were determined by XRD. The cross-section of CaZn based BGA immersion in Hank's solution for 10 days was also characterized by SEM and EDS mapping. The hydrogen evolution and the pH value of the solution were monitored during the soaking experiment. An average of three measurements was taken. The influence of corrosion on the integrity of mechanical property was also tested by compression test. After immersion in Hank's solution for 10 and 30 days, the 2 mm rods were removed, gently rinsed with absolute alcohol and distilled water sequently and dried at room temperature. The samples were tested on an Instron 5500R1186 machine for uniaxial compression.

2.4. Electrochemical measurements

The electrochemical measurements were conducted on an electrochemical workstation (CHI 650C) in the Hank's solution. A three-electrode set-up was used for the measurements. The counter and reference electrode was made of platinum and saturated calomel electrode (SCE) respectively. The tested samples cut from 1 mm thick plate, disposed same as above immersion test, were used as working electrode. The exposed area to the solution was 0.196 cm^2. All potentials were measured with respect to SCE. The potential dynamical measurements were carried out at a scan rate of 1 mV/s and the initial potential was 200 mV below the open circuit potential. The corrosion rate can be got from the polarization curve using Faraday's law [45]. Electrochemical impedance spectroscopy (EIS) analysis was carried out at corrosion potential with a perturbing signal of 5 mV over the frequency range 10^5–10^{-2} Hz. The surface morphologies and chemical composition of the samples after polarization were characterized by SEM and EDS.

2.5. Cytotoxicity test

Human osteosarcoma cells (MG63) were used to evaluate the cytocompatibility of the experimental alloys. They were cultured in minimum essential medium (MEM), 10% fetal bovine serum (FBS),

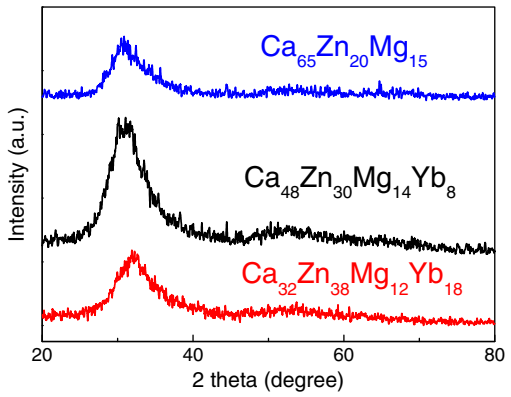

Fig. 1. XRD patterns of $Ca_{65}Zn_{20}Mg_{15}$, $Ca_{48}Zn_{30}Mg_{14}Yb_8$ and $Ca_{32}Zn_{38}Mg_{12}Yb_{18}$ BGAs.

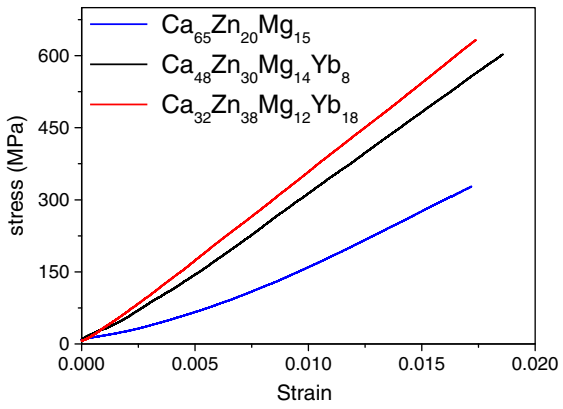

Fig. 3. The compression stress–strain curves of $Ca_{65}Zn_{20}Mg_{15}$, $Ca_{48}Zn_{30}Mg_{14}Yb_8$ and $Ca_{32}Zn_{38}Mg_{12}Yb_{18}$ BGAs.

100 U·ml^{-1} penicillin and 100 μg·ml^{-1} streptomycin at 37 °C in a humidified atmosphere of 5% CO_2. The samples used for cytotoxicity test were 1 mm thick plate. They were disposed in the above-mentioned way and sterilized by ultraviolet-radiation for at least 2 h prior to test.

According to the instruction of ISO 10993–5:1999, [46] extraction medium was prepared using MEM serum free medium with the surface area/extraction medium ratio 1 cm^2/mL in a humidified atmosphere with 5% CO_2 at 37 °C for 72 h and the extraction medium was stored at 4 °C before the cytotoxicity test. The control groups involved the use of MEM medium as negative control and 10% DMSO MEM medium as positive control. Cells were incubated in 96-well cell culture plates at 5×10^3 cells/100 μL medium in each well and incubated for 24 h to allow attachment. The medium was then replaced with 100 μl of extraction medium. After incubating the cells in a humidified atmosphere with 5% CO_2 at 37 °C for 1, 3 and 5 days, respectively, the 96-well cell culture plates were observed under an optical microscope. After that, 10 μL MTT was added to each well. The specimens were incubated with MTT for 4 h at 37 °C, and then 100 μL formazan solubilization solution (10% SDS in 0.01 M HCl) was added in each well for more than 10 h in the incubator in a humidified atmosphere. The spectrophotometrical absorbance of the specimens was measured by microplate reader (Bio-RAD680) at 570 nm with a reference wavelength of 630 nm.

Direct cytotoxicity was also performed by seeding 200 ml cell suspension onto the samples at a cell density of 5×10^4 cell/ml. After being cultured in a humidified atmosphere with 5% CO_2 at 37 °C for 1, 3 and 5 days in 96-well plates, the samples were fixed in 2.5% glutaraldehyde solution for 2 h at room temperature and rinsed 3 times with phosphate buffer solution (PBS, pH = 7.4), followed by

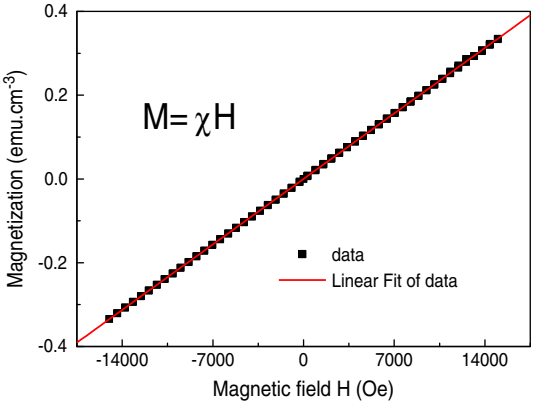

Fig. 4. The magnetization of $Ca_{32}Zn_{38}Mg_{12}Yb_{18}$ BGA as function of applied magnetic field at room temperature and the corresponding linear least square fit.

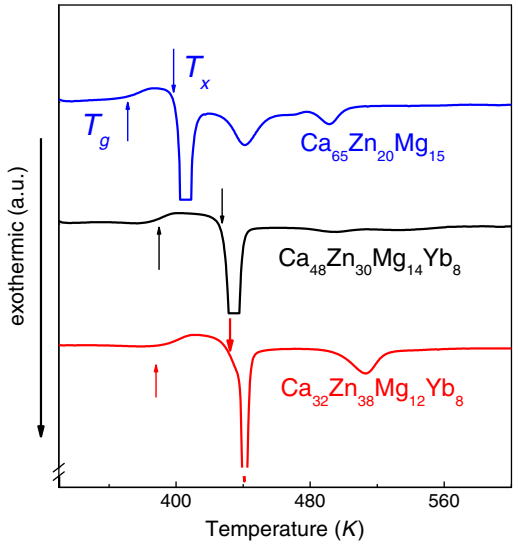

Fig. 2. DSC curves of $Ca_{65}Zn_{20}Mg_{15}$, $Ca_{48}Zn_{30}Mg_{14}Yb_8$ and $Ca_{32}Zn_{38}Mg_{12}Yb_{18}$ BGAs.

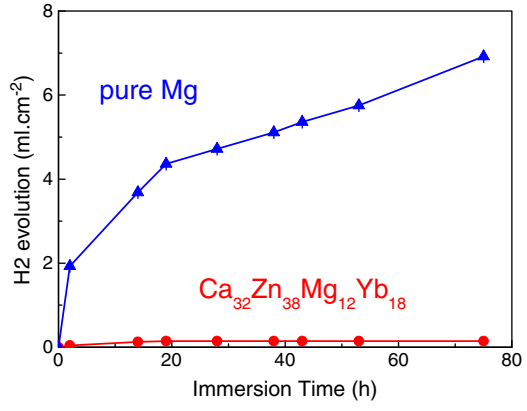

Fig. 5. The hydrogen evolution volume against immersion time of $Ca_{32}Zn_{38}Mg_{12}Yb_{18}$ BGA and pure Mg.

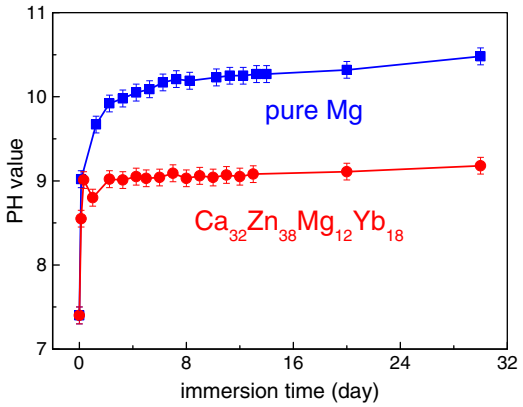

Fig. 6. The PH values against immersion time of $Ca_{32}Zn_{38}Mg_{12}Yb_{18}$ BGA and pure Mg.

dehydration in a gradient ethanol/distilled water mixture (50%, 60%, 70%, 80%, 90% and 100%) for 10 min each and dried in hexamethyldisilazane (HMDS) solution. The morphology of cell adhered experimental samples was observed by SEM. The concentrations of released Ca, Zn, Mg and Yb ions in the extraction medium were measured by ICP-AES (Leeman, Profile). The pH values were also measured for each experimental group.

3. Results

3.1. Structure, physical and mechanical properties

The Ca–Zn–Mg–Yb alloy shows good glass-forming ability in a wide composition range. Fig. 1 exhibits the XRD patterns of three representative alloys $Ca_{65}Zn_{20}Mg_{15}$, $Ca_{48}Zn_{30}Mg_{14}Yb_8$ and $Ca_{32}Zn_{38}Mg_{12}Yb_{18}$. There are only broad main peaks without detectable sharp peaks indicating the amorphous nature of these typical CaZn based alloys. The amorphous structure of the above mentioned alloys at room temperature is further confirmed by DSC curves. As shown in Fig. 2, all the experimental alloys show distinct glass transition and sharp crystallization peaks (at heating with a rate of 20 $K \cdot min^{-1}$) which are typical glassy features of the alloy. The values of glass transition temperature (T_g) of the $Ca_{65}Zn_{20}Mg_{15}$, $Ca_{48}Zn_{30}Mg_{14}Yb_8$ and $Ca_{32}Zn_{38}Mg_{12}Yb_{18}$ are 370 K, 382 K and 391 K, respectively. The crystallization temperature T_x, liquidus temperature T_l, supercooled liquid region $\Delta T = T_x - T_g$, and the reduced glass transition temperature[28] $T_{rg} = T_g/T_l$ are listed in

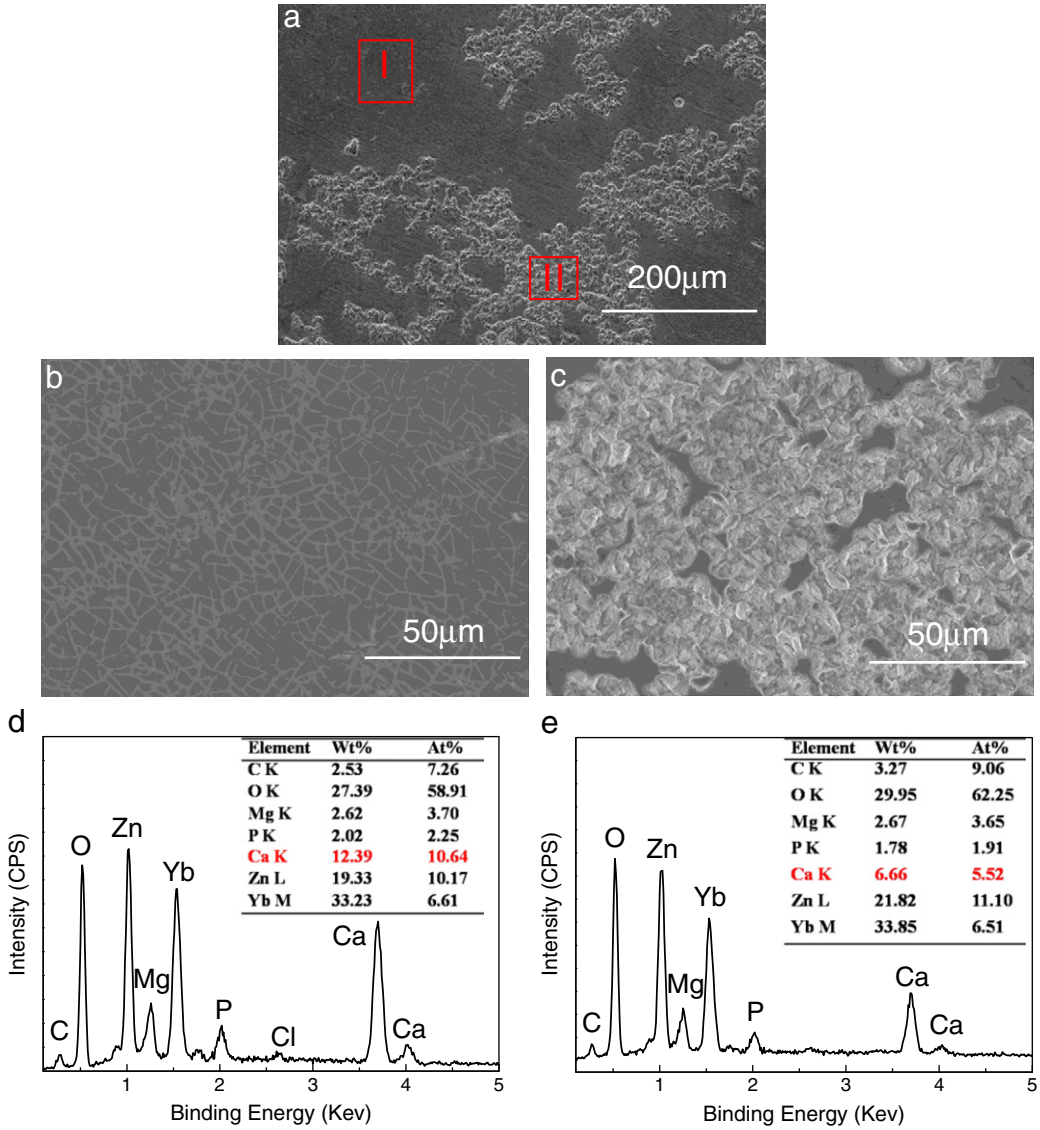

Fig. 7. (a) SEM images of $Ca_{32}Zn_{38}Mg_{12}Yb_{18}$ BGA after immersion in Hank's solution for 3 h. (b) High magnification image of the framed smooth zone I in (a), and (d) corresponding EDS spectra. (c) High magnification image of the framed rough zone II in (a), and (e) corresponding EDS spectrum.

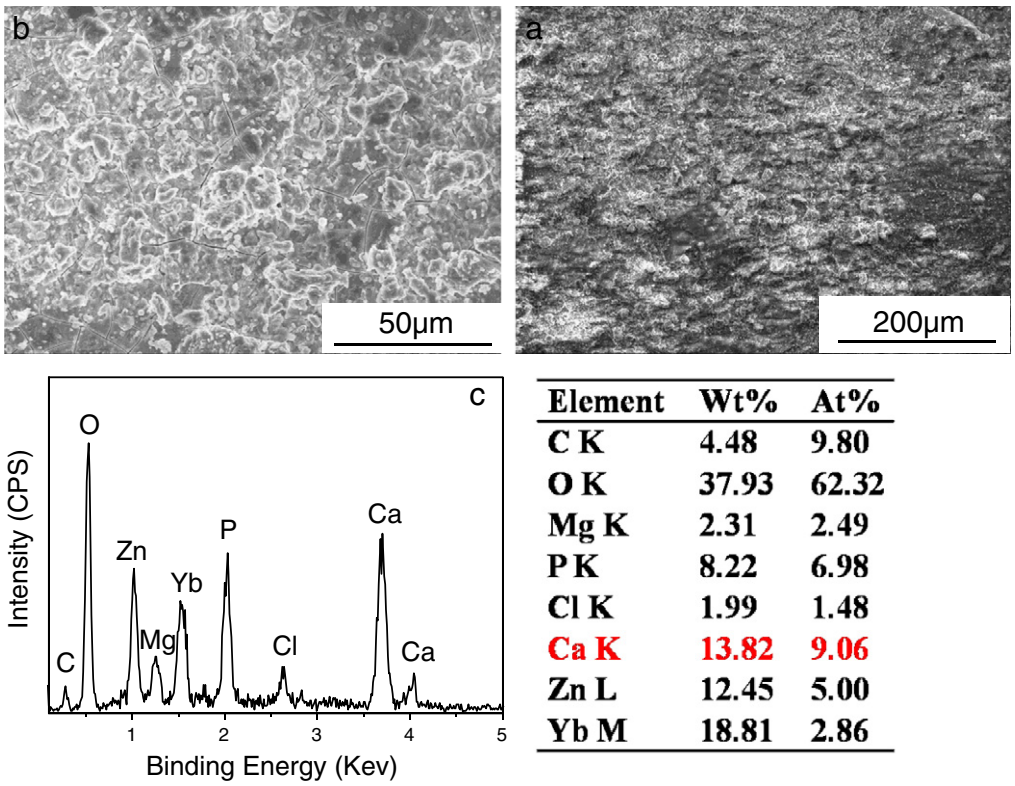

Element	Wt%	At%
C K	4.48	9.80
O K	37.93	62.32
Mg K	2.31	2.49
P K	8.22	6.98
Cl K	1.99	1.48
Ca K	13.82	9.06
Zn L	12.45	5.00
Yb M	18.81	2.86

Fig. 8. (a) SEM images of $Ca_{32}Zn_{38}Mg_{12}Yb_{18}$ BGA after immersion in Hank's solution for 30 days. (c) Corresponding EDS spectrum of the zone in (b).

Table 1. The T_g and T_x of these BGAs are much high than the body temperature indicating that the BGAs can sustain glassy state when is implanted into human body. With more zinc added, the T_g and T_x of the CaZn-based BGA increase monotonously.

The magnetization variation of $Ca_{32}Zn_{38}Mg_{12}Yb_{18}$ BGA under applied magnetic field at room temperature shown in Fig. 4 indicates that the glassy alloy is paramagnetic. It results from the diamagnetism of zinc and paramagnetism of other constitute elements. As magnetic susceptibility is the ratio between magnetization and the applied field, the magnetic susceptibility $\chi = M/H$, got from the slope through linear least square fit of the data is 22.3×10^{-6}, close to that of calcium 21.7×10^{-6}.

The compression stress–strain curves of the $Ca_{65}Zn_{20}Mg_{15}$, $Ca_{48}Zn_{30}Mg_{14}Yb_8$ and $Ca_{32}Zn_{38}Mg_{12}Yb_{18}$ BGAs are presented in Fig. 3. The elastic strain limits of the CaZn based BGA is about 2% similar to that of most other BGAs, and is much higher than that of their crystalline alloys (typically range between 0.1% and 0.5%). The values of fracture strength of $Ca_{65}Zn_{20}Mg_{15}$, $Ca_{48}Zn_{30}Mg_{14}Yb_8$ and $Ca_{32}Zn_{38}Mg_{12}Yb_{18}$ are 330 MPa, 607 MPa and 613 MPa, respectively; and the values of Young's modulus are 21 ± 2 GPa, 32 ± 2 GPa

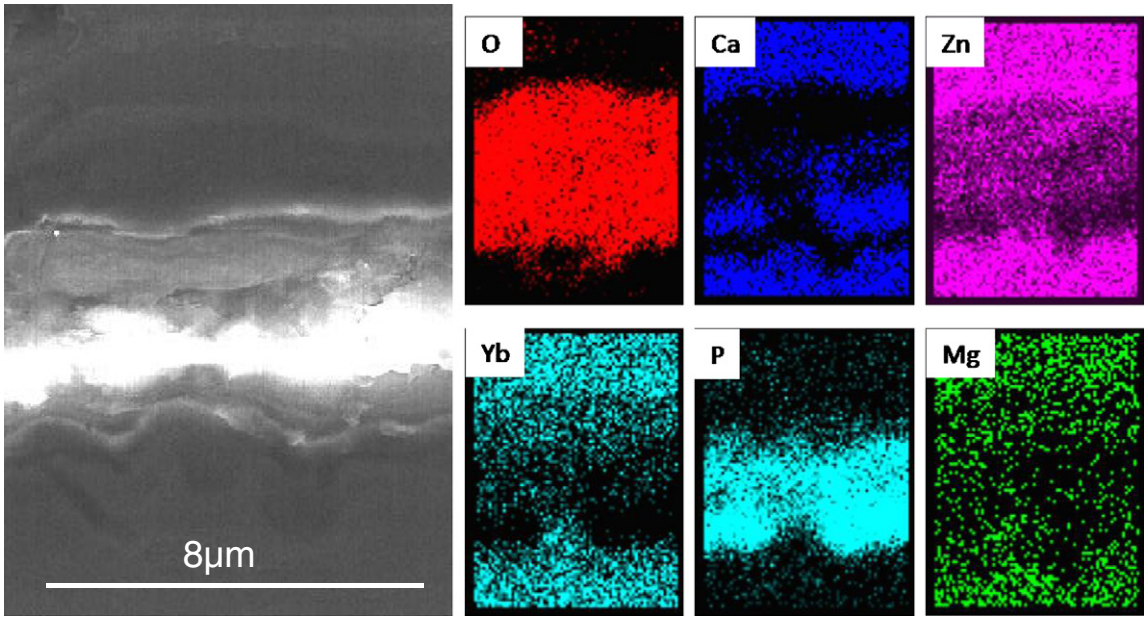

Fig. 9. SEM image and corresponding EDS maps of cross-section from stacks of $Ca_{32}Zn_{38}Mg_{12}Yb_{18}$ BGA immersed in Hank's solution for 10 days.

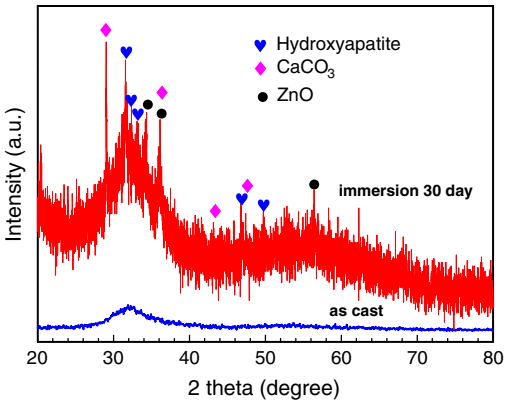

Fig. 10. XRD pattern of $Ca_{32}Zn_{38}Mg_{12}Yb_{18}$ BGA after immersion for 30 days.

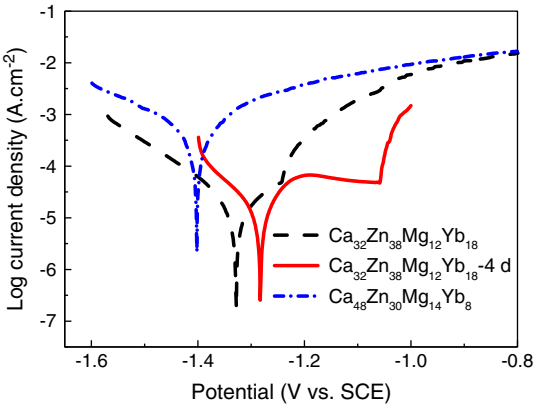

Fig. 12. Tafel curves of CaZn based BGAs tested in the Hank's solution. Where $Ca_{32}Zn_{38}Mg_{12}Yb_{18}$-4d represents that the test was carried out after $Ca_{32}Zn_{38}Mg_{12}Yb_{18}$ BGA was immersed in the Hank's solution for 4 days.

and 37 ± 2 GPa, respectively. The fracture strength and Young's modulus increase with zinc content increasing. This is due to the high Young's modulus of zinc (108 GPa), which is much higher than that of calcium (20 GPa). The more content of zinc is, the higher fracture strength and Young's modulus of the CaZn based BGA are. The result is consistent with the correlation between properties of BGA and the elastic constants of constitute elements [47]. Because of the wide glass-formation composition region for the experimental alloy, it is possible to modulate the value of fracture strength and Young's modulus by varying the atomic ratio of calcium and zinc. The density of $Ca_{32}Zn_{38}Mg_{12}Yb_{18}$ alloy is 4.194 g/cm^3.

3.2. Immersion results

The hydrogen evolution volume over immersion time of the experimental alloys is shown in Fig. 5. Obviously, the hydrogen release rate of $Ca_{32}Zn_{38}Mg_{12}Yb_{18}$ BGA is much smaller than that of pure Mg. After immersion for 38 h, hardly any hydrogen is newly formed for the BGA. The PH values of the BGA and pure Mg as functions of immersion time are presented in Fig. 6. It can be seen that accompanying with the hydrogen release the PH values increase rapidly as samples were immersed in the solution. But the PH value of $Ca_{32}Zn_{38}Mg_{12}Yb_{18}$ gradually gets stable in next 2 days, and then the corrosion becomes steady. During the immersion period, the $Ca_{32}Zn_{38}Mg_{12}Yb_{18}$ BGA shows a lower PH value. After immersion in Hank's solution for 30 days, the PH values are 9.18 and 10.48 for the $Ca_{32}Zn_{38}Mg_{12}Yb_{18}$ BGA and pure Mg, respectively.

The surface morphologies and corresponding chemical composition of the $Ca_{32}Zn_{38}Mg_{12}Yb_{18}$ BGA immersed in Hank's solution for 3 h are shown in Fig. 7(a)–(e). A portion of the surface was still flat with shallow cracks presented in Fig. 7(b), which may be caused by dehydration after removing from the solution [48]. While as shown in Fig. 7(c), the weak regions of sample surface suffered from corrosion under the attack of chloride and other ions in the solution, the outmost layer dissolved gradually, and exhibited rough surface. The EDS result of smooth zone is shown in Fig. 7(d). It can be seen that the main composition is C, O, Mg, P, Ca, Zn and Yb. In contrast, relatively low calcium atomic ratio is found in the rough zone as presented in Fig. 7(e), indicating that Ca had firstly released from the surface. The surface morphology and composition of $Ca_{32}Zn_{38}Mg_{12}Yb_{18}$ BGA immersed in Hank's solution for 30 days are shown in Fig. 8(a)–(c). A nearly uniform corrosion product is deposited on the sample surface. The EDS data reveal that the corrosion surface is depleted of Ca and Mg, while Zn, Yb and especially O, P are abundant in the passive film.

Fig. 9 shows the SEM image of cross-section and corresponding EDS maps from stacks of $Ca_{32}Zn_{38}Mg_{12}Yb_{18}$ BGA after immersion for 10 days. It shows that a contact corrosion layer about 3 μm was formed. According to the micrograph and corresponding EDS maps, it is reasonable to speculate that the corrosion layer can be divided into two sublayers. The outmost layer which is the bright phase presented in SEM image is rich in Ca, P and O, and the subjacent layer, conversely, is depleted of Ca and P, while Zn, Yb and especially O are abundant. The XRD pattern of $Ca_{32}Zn_{38}Mg_{12}Yb_{18}$ after immersion for 30 days is shown in Fig. 10. There are two obvious humps with several sharp diffraction peaks. The diffraction hump may origin from the precipitation[17] or the BGA substrate. The diffraction peaks corresponding to the corrosion products are determined to be Hydroxyapatite, ZnO and $CaCO_3$.

The compression curves of $Ca_{32}Zn_{38}Mg_{12}Yb_{18}$ BGA after degradation in Hank's solution for 10 days and 30 days are shown in Fig. 11. The compression fracture strength did not show obvious decline, clearly superior to Mg–6Zn alloy which exhibits a large decrease in bending strength resulting from surface defects such as holes formed during non-uniform corrosion [17]. After immersion in Hank's

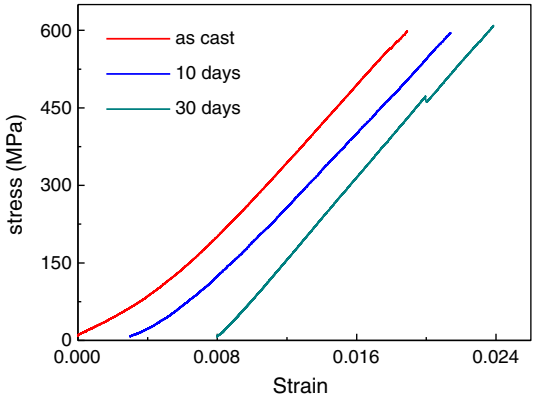

Fig. 11. Stress–strain curves of $Ca_{32}Zn_{38}Mg_{12}Yb_{18}$ BGA after immersion in Hank's solution for various times.

Table 2
Electrochemical parameters of CaZn based BGAs and pure Mg [16] obtained from potential dynamical polarization curves.

Sample	Corrosion potential E_{corr}(V)	Corrosion current density i_{corr}(μA/cm^2)
Mg	−1.533	15.98
$Ca_{48}Zn_{30}Mg_{14}Yb_8$	−1.401	415
$Ca_{32}Zn_{38}Mg_{12}Yb_{18}$	−1.329	10.2
$Ca_{32}Zn_{38}Mg_{12}Yb_{18}$ immersion 4 days	−1.281	9.9

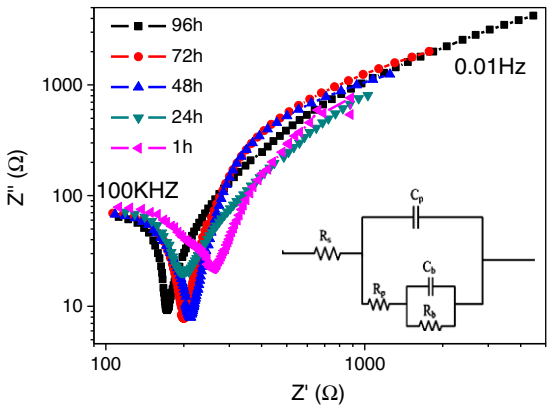

Fig. 13. Nyquist plots of $Ca_{32}Zn_{38}Mg_{12}Yb_{18}$ BGA (the imaginary part of the impedance vs. the real part, in a log–log representation). The inset is the equivalent circuit for fitting Nyquist plots.

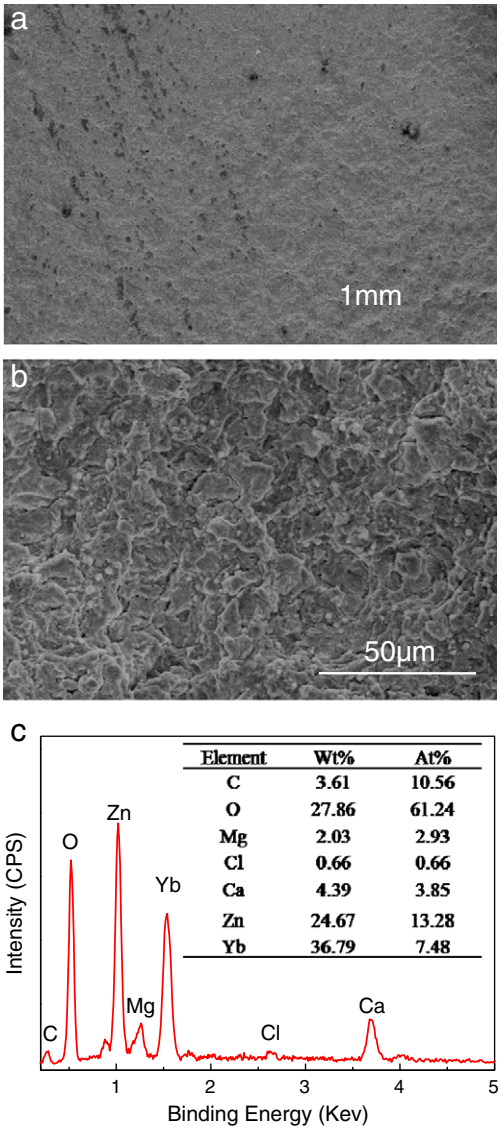

Fig. 14. SEM images of surface morphology of $Ca_{32}Zn_{38}Mg_{12}Yb_{18}$ BGA after polarized in Hank's solution (a) low magnification image (b) High magnification image and (c) EDS spectrum corresponding to area in (b).

solution at 37 °C for 30 days, the Young's modulus of the BGA increased slightly due to the structural relaxation at 37 °C for 30 days.

3.3. Electrochemical measurements

The potential dynamical polarization curves of CaZn based BGAs are shown in Fig. 12. The corresponding electrochemical parameters obtained from the curves are presented in Table 2. After alloying with zinc and ytterbium, the corrosion potentials E_{corr} of the CaZn based BGAs are much higher than that of Ca (−3.11 Ca/Ca^{2+} vs. SCE), even nobler than that of Mg (−1.824 Mg/Mg^{2+} Vs. SCE). After immersion in Hank's solution for 4 days, the corrosion potential E_{corr} of $Ca_{32}Zn_{38}Mg_{12}Yb_{18}$ BGA shifts towards positive direction.

The corrosion current density value of $Ca_{32}Zn_{38}Mg_{12}Yb_{18}$ BGA is only 9.9 μA/cm^2, much smaller than that of pure Mg (15.98 μA/cm^2) [16]. Whereas, the value for $Ca_{48}Zn_{30}Mg_{14}Yb_8$ BGA is one order in magnitude higher than that of Mg. The anodic polarization curve of $Ca_{32}Zn_{38}Mg_{12}Yb_{18}$ shows passivation like behavior compared with $Ca_{48}Zn_{30}Mg_{14}Yb_8$ BGA, which undergone active corrosion. This means that high content of Zn and Yb can facilitate protective film formation and decrease the corrosion current. After immersing the sample in Hank's solution for 4 days, the passivation region in the potential dynamical polarization curve of $Ca_{32}Zn_{38}Mg_{12}Yb_{18}$ BGA become longer, about 0.222 V, indicating that formed corrosion layer can act as protective film on the surface. This is also supported by the electrochemical impedance spectroscopy (EIS) shown in Fig. 13. The Nyquist plots of $Ca_{32}Zn_{38}Mg_{12}Yb_{18}$ BGA presented a complex two-semicircle-like shape with two time constants like Mg-based bulk metallic glass [9], the equivalent circuit is shown in the inset of Fig. 13. The corrosion resistance increases as function of the immersion time in the first 96 h, and the impedance values obtained from the fitting range from 600 to 6400 Ω.

The SEM micrographs and chemical composition of $Ca_{32}Zn_{38}Mg_{12}Yb_{18}$ BGA after polarization testing in Hank's solution are shown in Fig. 14. A rough surface with shallow pockmarks can be seen in the images [see Fig. 14(a)–(b)]. The EDS spectrum corresponding to area in Fig. 14(b) is presented in Fig. 14(c). Compared to the nominal composition of $Ca_{32}Zn_{38}Mg_{12}Yb_{18}$ BGA, it is obviously that the corrosion surface is depleted of Ca and Mg, while Zn, Yb and especially O are abundant in the passive film.

3.4. Cytotoxicity assessment

According to above corrosion result, $Ca_{32}Zn_{38}Mg_{12}Yb_{18}$ BGA is selected to do further cytotoxicity assessment by indirect and direct methods. Fig. 15 presents the viability of MG 63 cells cultured in 5%, 10%, 50% and 100% $Ca_{32}Zn_{38}Mg_{12}Yb_{18}$ BGA glassy alloy extraction for

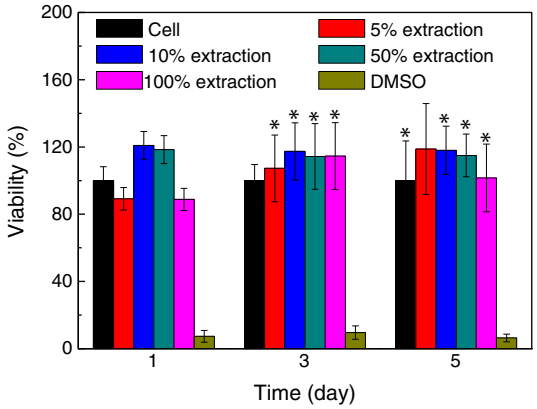

Fig. 15. The viability of MG63 cells cultured in different concentration of $Ca_{32}Zn_{38}Mg_{12}Yb_{18}$ BGA extraction (5%, 10%, 50% and 100%) and DMSO for different time (1, 3 and 5 days). (*$p>0.05$).

1, 3 and 5 days. Compared to the cell group, the viability of all cultured in extraction is better than 90%, similar to that of the negative group. There was no significant difference ($p>0.05$) between MG63 cells cultured in extracts and negative group. According to ISO 10993–5:1999[46], the grade of cytotoxicity of extract is 0–1 indicating that CaZn based BGA indeed shows biocompatibility to MG63 cells. The morphologies for MG63 cells cultured in 5%, 10%, 50% and 100% $Ca_{32}Zn_{38}Mg_{12}Yb_{18}$ BGA extract for 5 days is shown in Fig. 16. All of them presented healthy elongated spindle shape. This further confirms that the $Ca_{32}Zn_{38}Mg_{12}Yb_{18}$ BGA has good cytocompatibility with no negative effects on cell morphology and viability.

Based on above high cell viability on extract, direct contact test was carried out. The morphology of MG63 cells cultured on $Ca_{32}Zn_{38}Mg_{12}Yb_{18}$ BGA and pure Mg substrate for 3 days is presented in Fig. 17. MG63 cells cultured on $Ca_{32}Zn_{38}Mg_{12}Yb_{18}$ BGA substrate are still in healthy elongated spindle shape as shown in Fig. 17(a). Fig. 17(b) provides a clear view of MG63 cell which shows a polygonal shape firmly attached and spread well on the substrate surface. Whereas MG63 cells after incubation on pure Mg substrate revealed round shape in unhealthy state in Fig. 17(c).

The concentration of element release from $Ca_{32}Zn_{38}Mg_{12}Yb_{18}$ BGA and pure Mg in culture medium with MG63 cells for 1, 3 and 5 days are shown in Fig. 18. Compared to pure Mg, the concentration of Mg released from $Ca_{32}Zn_{38}Mg_{12}Yb_{18}$ BGA is two orders of magnitude lower. The highest element release from $Ca_{32}Zn_{38}Mg_{12}Yb_{18}$ BGA is Ca, the next is Mg, which is consistent with the sequence of ions in body solution. The PH values for $Ca_{32}Zn_{38}Mg_{12}Yb_{18}$ BGA and pure Mg cultured in MEM with MG63 cells variation over immersion time are recorded in Fig. 19. It is shown that the PH value slightly increases with the prolonged immersion time. The PH value for $Ca_{32}Zn_{38}Mg_{12}Yb_{18}$ BGA is much smaller and closer to initial value compared to that for pure Mg.

4. Discussion

The CaZn based BGA is a newcomer in biodegradable materials family. We have evaluated the feasibility of CaZn based BGA as biodegradable materials from the aspect of mechanical properties, magnetic susceptibility, corrosion behavior and biocompatibility according to the generalized request for biodegradable metal.[10,31] Next, we will compare CaZn based BGA with commonly investigated biomedical metals and alloys, especially Mg alloys and propose a schematic corrosion process to interpret the good corrosion resistance and cytocompatibility of the CaZn based BGAs.

4.1. Mechanical and physical properties

The combination of high fracture strength and fracture toughness makes metals more suitable for load-bearing applications compared with ceramics or polymeric materials, [9,30] so does the CaZn based BGA. Compared to conventional crystalline alloys, the BGAs possess high fracture strength and elastic strain limit, relatively low elastic constants. The Young's modulus of calcium is 20 GPa, which matches well with cortical bone. By alloying zinc, not only oxidation and corrosion resistances have been improved greatly, the fracture strength has also been improved. The fracture strengths versus elastic constants of the CaZn based BGA and present commonly investigated biomedical materials [8,9,21,31] are presented in Fig. 20. Compared to biomedical polymer, like PLA and PGA, the fracture strength of CaZn based BGA is 1–5 times higher. Besides, the released Ca from CaZn based BGA may improve the healing rate of the fractured bone. Compared to bioceramic and biomedical metallic materials, the Young's modulus of the CaZn based BGA is much closer to cortical bone. The low elastic modulus may minimize the stress shielding and facilitate load transfer to the surrounding bone [30]. The combining properties of the CaZn based BGA indicate that the alloy has great potential to be used as biomedical material.

One shortcoming for stainless steels, Co–Cr alloys and titanium alloys for biomedical application is that they may interfere with MRI diagnosis, [49] which can obtain various cross-sectional views and diagnose with no invasion and no exposure of the human body to X-ray radiation. Since metallic implants magnetize in the magnetic field of the MRI instrument and produce a distortion or blooming in the MRI image [26,50]. Magnetic susceptibility is an effective indicator for the amount of distortion of medical MRI image [26]. Fig. 21 shows the magnetic susceptibility of $Ca_{32}Zn_{38}Mg_{12}Yb_{18}$ and previously reported alloys used as biomedical devices [26,50]. The magnetic susceptibility

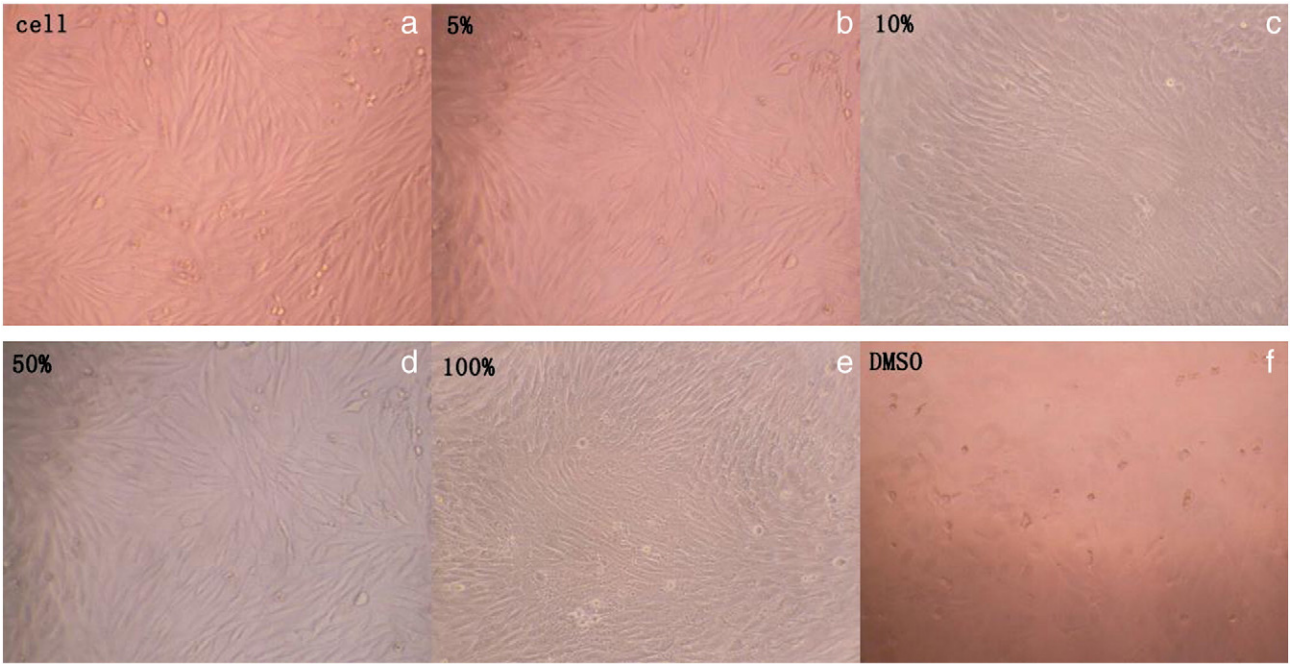

Fig. 16. Optical morphologies of MG63 cells cultured in (a) negative control, (b) 5%, (c) 10%, (d) 50%, (e) 100% $Ca_{32}Zn_{38}$ BGA extract and (f) positive control for 5 days.

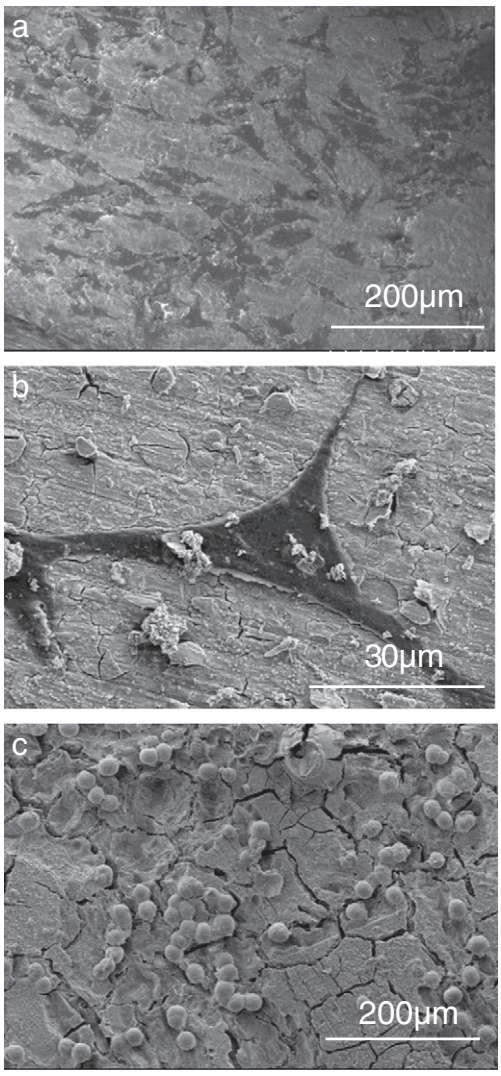

Fig. 17. The morphologies of MG63 cells directly cultured on $Ca_{32}Zn_{38}Mg_{12}Yb_{18}$ BGA (a) low magnification image (b) High magnification image (c) pure Mg for 3 days.

of $Ca_{32}Zn_{38}Mg_{12}Yb_{18}$ is much smaller than that of commonly used biomedical alloys, nearly one-tenth of that of Ti. According to MRI magnetic compatibility categorized by Schenck, the CaZn glassy alloy is located at the region of the first class but close to the boundary of the second class [50]. This means that bone graft substitutes made of CaZn based glassy alloy may produce limited image distortion or blooming in the MRI image compared to commonly used biomedical alloys.

4.2. Biocorrosion property

The main obstacle of Mg alloys for biodegradable application is high degradation rate and consequent loss of the mechanical integrity. Fig. 22 shows the corrosion rate of $Ca_{32}Zn_{38}Mg_{12}Yb_{18}$ BGA and as-reported Mg alloys determined from Tafel extrapolation using Faraday's law: corrosion rate (mm/year) $= 3.27\times10^{-3}$ $(Mi_{corr})/\rho n$, where M (g/mol), n, and ρ (g/cm^3) are atomic-fraction-weighted values of the atomic weight, ion valence, and density for the alloy elements, respectively, and i_{corr} (μA/cm^2) is the corrosion current density obtained from Tafel method [45]. It can be seen that the degradation rate of $Ca_{32}Zn_{38}Mg_{12}Yb_{18}$ in Hank's solution is slower than that of reported various biomedical Mg alloys [16,22,51] presented in Fig. 22. The low degradation rate is due to the high content of corrosion resistance Zn and Yb in the alloy. Zinc benefits the

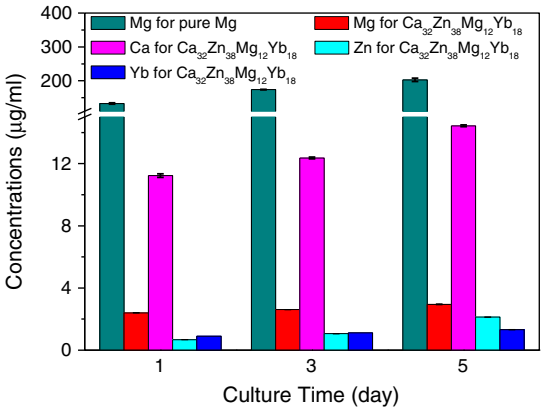

Fig. 18. The concentration of element release from $Ca_{32}Zn_{38}Mg_{12}Yb_{18}$ BGA and pure Mg in culture medium with MG63 cells for 1, 3 and 5 days.

corrosion film formation [17] and zinc oxide/hydroxide are the important constitutes of protective layer [31]. This is validated by the EDX maps of cross-section of $Ca_{32}Zn_{38}Mg_{12}Yb_{18}$ BGA, as Zn and O are abundant adjacent to the alloy matrix as shown in Fig. 9. Ytterbium, as a kind of heavy rare earth elements has beneficial effect on the corrosion resistance of Mg matrix as previously reported in Mg alloy [18]. Another reason for the low degradation rate is due to the glassy structure. Different from conventional crystalline Mg alloys, the CaZn based BGA can alloy high content of Zn exceeding its solid solubility in calcium according to Ca–Zn phase diagram, and especially, the alloy is still homogeneity in concentration and structure. This can reduce galvanic corrosion effectively, which usually happens in multiphase alloys with different corrosion potentials.

The schematic in vitro corrosion process of the CaZn based BGA is shown in Fig. 23. As the CaZn based BGA immerse in Hank's solution, the surface is exposed to the aqueous solution, especially under the attack of Cl^-, anodic reaction $(M(s)\rightarrow M^{n+}(aq)+ne^-)$ taken place at the weak regions, and corresponding cathode reaction$(2H_2O+2e^-\rightarrow H_2+2OH^-\ (aq))$also occurs, which lead the region adjacent to the interface between the sample and solution significantly alkalized. According to the morphology and corresponding constitute of $Ca_{32}Zn_{38}Mg_{12}Yb_{18}$ alloy after immersion in Hank's solution for 3 h shown in Fig. 7, the calcium firstly releases from the matrix. The released cations are soon combined with OH^- and hydroxide precipitated on the surface. As existence of Cl^- can destroy the equilibrium of $Mg(OH)_2$ between precipitation and dissolution, [5] the formed hydroxides layer is unstable, especially for $Ca(OH)_2$. The released cations are also precipitated in the form of phosphates and carbonates for HPO_4^{2-}, $H_2PO_4^-$, PO_4^{3-}, CO_3^{2-} and HCO_3^- existed in the

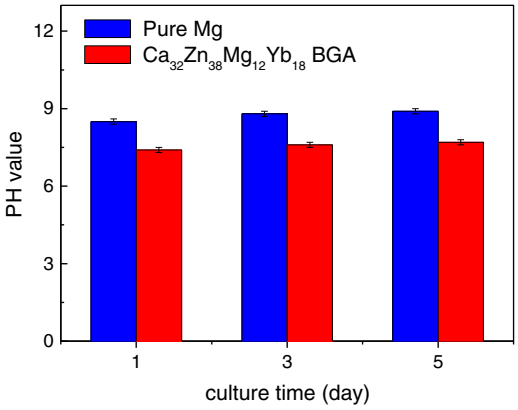

Fig. 19. The PH value for $Ca_{32}Zn_{38}Mg_{12}Yb_{18}$ BGA and pure Mg cultured in MEM with MG63 cells variation over immersion time.

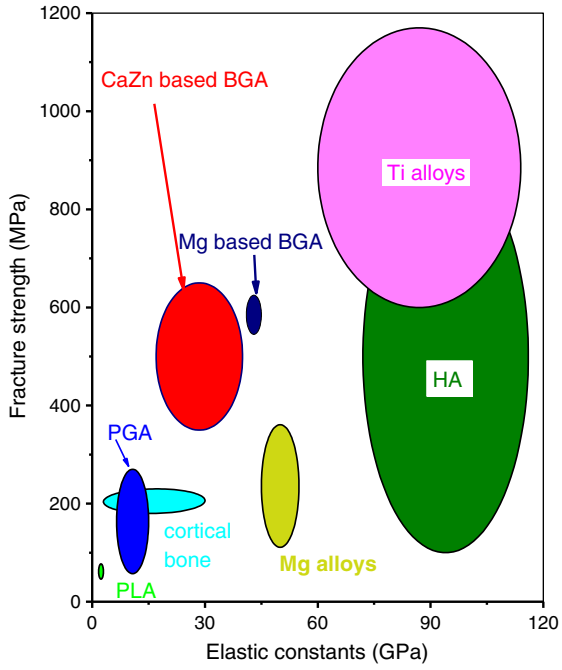

Fig. 20. Fracture strength vs. elastic constants data of CaZn based BGA and present commonly investigated biomedical materials [8,9,21,31].

solution. Furthermore, the solubility product constant K_{sp} of $Ca_3(PO_4)_2$ (2.07×10^{-33}) and $CaCO_3$ (3.36×10^{-9}) is much smaller than that of $Ca(OH)_2$ (5.02×10^{-6}), [52] which would stimulate the dissolution of the hydroxide layer. As the corrosion proceeded, calcium is depleted from the region adjacent to the surface gradually and most precipitated as phosphates and carbonates at the outmost layer, which is confirmed by the results of EDS mapping in Fig. 9 and XRD pattern in Fig. 10. Simultaneously, the PH value is increased, which benefits ZnO and $Yb(OH)_3$ formation according to the Pourbaix diagram of Zn and Yb [9,53]. Subsequently, the corrosion resistance is obviously improved. After immersion in Hank's solution for 38 h, hardly any hydrogen was newly formed.

4.3. Biocompatibility

Biocompatibilty is another important request for biomedical metal. Simply, to guarantee the biosafety, the selected constitute elements are either essential to human body, such as Ca, Mg and Zn,

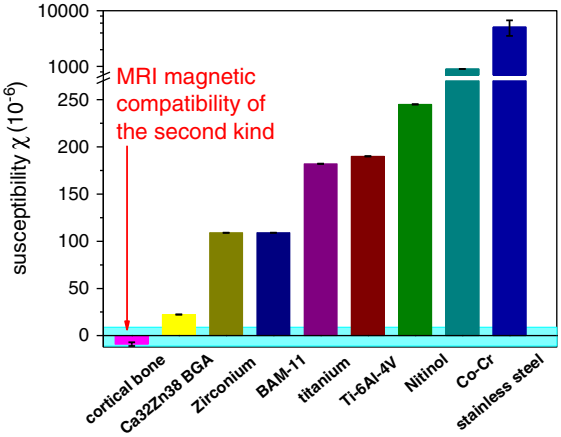

Fig. 21. The comparison of magnetic susceptibility of $Ca_{32}Zn_{38}Mg_{12}Yb_{18}$ BGA with previously reported biomedical metals [26,50]. The dark region represents the range of MRI magnetic compatibility of the second kind.

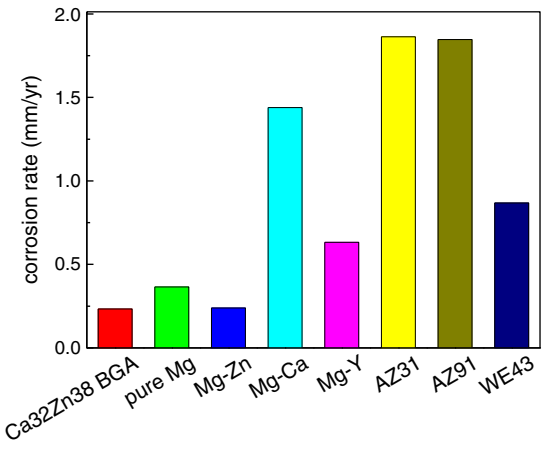

Fig. 22. Comparison corrosion rate of $Ca_{32}Zn_{38}Mg_{12}Yb_{18}$ BGA with reported Mg alloys [16,22,51] determined from Tafel extrapolation.

[21] or have been used in Mg alloys and shown good biocompatibility for animal tests like rare earth element, Yb [4,37].

Cytotoxicity is the preliminary stage to evaluate the biocompatibility of a new material. The CaZn based BGA is intended to be used as bone graft substitutes. Therefore, in vitro biocompatibility assessment is using Human osteoblast-like (MG63) cell lines, which can stimulate the interactions between implants and tissue cells to some extent. The indirect cytotoxicity of the CaZn based BGA is Grades 0–1, according to ISO 10993–5:1999, [46] indicating that this kind of glassy alloy shows biosafety for biomedical application, which is further verified by direct cytotoxicity assay.

It is known that cells are very sensitive to the environment [31]. From the viewpoint of morphologies of MG63 cells directly incubated on the sample surface, the cytocompatibility of the CaZn based BGA is superior compared to pure Mg. Firstly, this may be assigned to the released ions. According to evaluation carried out by Feyerabend et al., [38,54] when the concentration of Mg, Ca, heavy rare earth element is 2 mM/L, 10 mM/L and 1 mM/L, respectively, and the viability of MG63 cells is nearly comparable to control group. As reported by Popp et al., [55] zinc doesn't show significant effect on cell number and alkaline phosphate activity of rat bone marrow stromal cells cultured in osteogenic medium supplemented Zn^{2+} concentrations of 4×10^{-5} M for up to 3 weeks. The concentration of element released from $Ca_{32}Zn_{38}Mg_{12}Yb_{18}$ BGA shown in Fig. 18 is smaller than the above value, especially for Mg, Ca and Yb which are one to two orders in magnitudes smaller. But the concentration of Mg released from pure Mg is two to three times higher. From the results of immersion or electrochemical corrosion, the degradation rate of $Ca_{32}Zn_{38}Mg_{12}Yb_{18}$ alloy is slower than that of pure Mg. Consequently, the hydrogen evolution rate and PH value of $Ca_{32}Zn_{38}Mg_{12}Yb_{18}$ BGA is smaller, which is another reason for the superior direct cytocompatibility. Furthermore, referring to the result reported by Paul et al., the osteoblast-like MG63 cells spread completely on calcium zinc magnesium phosphate surface are comparable to that on hydroxypatite after cultured for 5 days, [56] because the outmost corrosion layer is relatively rich in Ca, P and O as well as the corrosion resistance layer underneath that layer. The cells growth and differentiation are promoted by the calcium and other cations (such as Mg, Zn,Yb) phosphate corrosion layer, and the degradation rate is then slowed down by ZnO and hydroxides as shown in Fig. 23. Whereas, MG63 cells contact directly on $Mg(OH)_2$ for pure Mg.

5. Conclusions

We have successfully developed the CaZn based BGAs which have potential to be used as biodegradable bone graft substitutes.

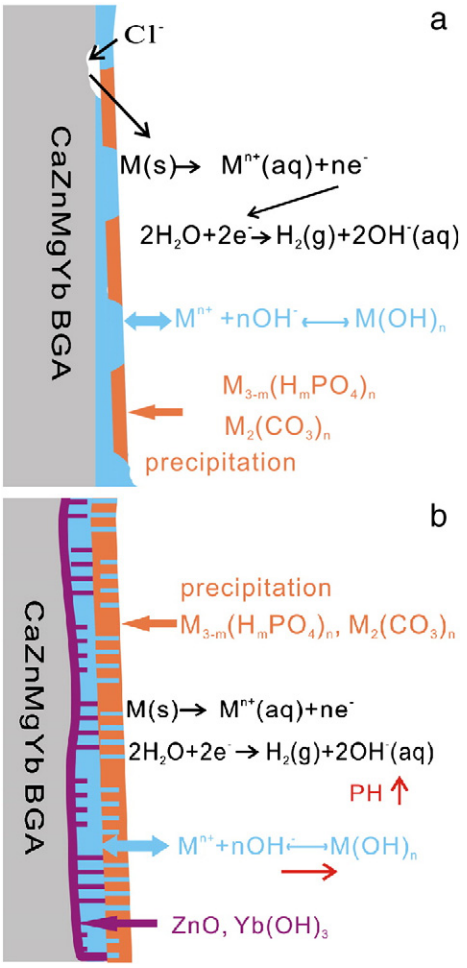

Fig. 23. Schematic corrosion process of CaZn based BGA, where M^{n+} is Ca^{2+}, Mg^{2+}, Zn^{2+} and Yb^{2+}. (a) Initial state. (b) Stable state.

Compared to commonly investigated biomedical metal, the new class of biodegradable CaZn based BGAs presents the merits, such as low Young's modulus matches with cortical bone, high fracture strength which is two to three times that of pure Mg, low magnetic susceptibility which is compatible with MRI diagnosis, and high corrosion resistance and good cytocompatibility. The glassy alloy also has low hydrogen release rate when immersed in Hank's solution. The very low degradation rate is due to the formation of the ZnO and hydroxides layers adjacent to the CaZn based BGA matrix. The cell growth and differentiation can also be promoted by calcium and other cations (such as Mg, Zn,Yb) phosphates in the outmost corrosion layer. The new class of biodegradable CaZn based BGAs would enrich the family of biomaterials.

Acknowledgment

Experimental assistance and discussions of D.Q. Zhao, L. Huang and R. Li are appreciated. Financial support is from the NSF of China (Nrs. 50731008 and 50921091) and MOST 973 of China (No. 2007CB613904 and 2010CB731600).

References

[1] Y.H. Yun, X.F. Guo, Mater. Today 12 (2009) 22.
[2] H. Hermawan, D. Dube, D. Mantovani, Acta Biomater. 6 (2010) 1693.
[3] F. Witte, Acta Biomater. 6 (2010) 1680.
[4] R. Erbel, C.D. Mario, J. Bartunek, J. Bonnier, D.B. Bruyne, F.R. Eberli, Lancet 369 (2007) 1869.
[5] Z.J. Li, X.N. Gu, S.Q. Lou, Y.F. Zheng, Biomaterials 29 (2008) 1329.
[6] M.B. Kannan, R.K.S. Raman, Biomaterials 29 (2008) 2306.
[7] F. Witte, V. Kaese, H. Haferkamp, E. Switzer, A. Meyer-Lindenberg, C.J. Wirth, Biomaterials 26 (2005) 3557.
[8] A.M. Pietak, M.P. Staiger, J. Huadmai, G. Dias, Biomaterials 27 (2006) 1728.
[9] B. Zberg, P.J. Uggowitzer, J.F. Loffler, Nat. Mater. 8 (2009) 887.
[10] B. Liu, Y.F. Zheng, Acta Biomater. 7 (2011) 1407.
[11] M. Peuster, P. Wohlsein, M. Brugmann, M. Ehlerding, K. Seidler, C. Fink, Heart 86 (2001) 563.
[12] L.P. Xu, F. Pan, G.L. Yu, L. Yang, E.L. Zhang, K. Yang, Biomaterials 30 (2009) 1512.
[13] L.C. Li, J.C. Gao, Y. Wang, Surf. Coat. Technol. 185 (2004) 92.
[14] X.N. Gu, W. Zheng, Y. Cheng, Y.F. Zheng, Acta Biomater. 5 (2009) 2790.
[15] H.M. Wong, K.W.K. Yeung, K.O. Lam, V. Tam, P.K. Chu, K.D.K. Luk, Biomaterials 31 (2010) 2084.
[16] X.N. Gu, Y.F. Zheng, Y. Cheng, S.P. Zhong, T.F. Xi, Biomaterials 30 (2009) 484.
[17] S.X. Zhang, X.N. Zhang, C.L. Zhao, J.A. Li, Y. Song, C.Y. Xie, et al., Acta Biomater. 6 (2010) 626.
[18] N. Hort, Y. Huang, D. Fechner, M. Stormer, C. Blawert, F. Witte, Acta Biomater. 6 (2010) 1714.
[19] M. Bohner, Mater. Today 13 (2010) 24.
[20] F. Wu, J. Wei, H. Guo, F.P. Chen, H. Hong, C.S. Liu, Acta Biomater. 4 (2008) 1873.
[21] J.Z. Ilich, J.E. Kerstetter, J. Am. Coll. Nutr. 19 (2000) 715.
[22] X.N. Gu, Y.F. Zheng, Front Mater. Sci. China 4 (2010) 111.
[23] A. Sigel, H. Sigel, Metal ions in biological systems, Metal Ions and Their Complexes in Medication, Volume 41, FontisMedia S.A. and Marcel Dekker, Inc, 2004, p. 122.
[24] F. Bronner, Dent. Clin. North Am. 47 (2003) 209.
[25] A.M. James, M.P. Lord, London: Macmillan;1992.
[26] J.A. Horton, D.E. Parsell, in: T. Egami, A.L. Greer, A. Inoue, S. Ranganathan (Eds.), Supercooled Liquids, Glass Transition and Bulk Metallic Glasses Symposium, 2003, p. 179.
[27] J. Schroers, G. Kumar, T.M. Hodges, S. Chan, T.R. Kyriakides, JOM 61 (2009) 21.
[28] W.H. Wang, Adv. Mater. 21 (2009) 4524;
Q. Luo, W.H. Wang, J. Non-cryst. Solids 355 (2009) 759;
S. Li, R.J. Wang, M.X. Pan, D.Q. Zhao, W.H. Wang, J. Non-cryst. Solids 354 (2008) 1080.
[29] L. Huang, Z. Cao, H.M. Meyer, P.K. Liaw, E. Garlea, J.R. Dunlap, Acta Biomater. 7 (2011) 395.
[30] M.D. Demetriou, A. Wiest, D.C. Hofmann, W.L. Johnson, B. Han, N. Wolfson, JOM 62 (2010) 83.
[31] X.N. Gu, Y.F. Zheng, J.Q. Wang, W.H. Wang, Biomaterials 31 (2010) 1093.
[32] L. Liu, C.L. Qiu, Q. Chen, K.C. Chan, S.M. Zhang, J. Biomed. Mater. Res. A 86A (2008) 160.
[33] O.N. Senkov, D.B. Miracle, V. Keppens, P.K. Liaw, Metall. Mater. Trans. A 39 (2008) 1888.
[34] W. Jiao, K. Zhao, X.K. Xi, W.H. Wang, J. Non-Cryst. Solids 356 (2010) 1867.
[35] H.F. Li, Y.B. Wang, Y. Cheng, Y.F. Zheng, Mater. Lett. 64 (2010) 1462.
[36] M. Yamaguchi, H. Oishi, Y. Suketa, Biochem. Pharmacol. 35 (1987) 4007.
[37] F. Witte, J. Fischer, J. Nellesen, H.A. Crostack, V. Kaese, A. Pisch, Biomaterials 27 (2006) 1013.
[38] A. Drynda, N. Deinet, N. Braun, M. Peuster, J. Biomed. Mater. Res. A 91 (2009) 360.
[39] W.H. Wang, Prog. Mater. Sci. 52 (2007) 540;
W.H. Wang, C. Dong, C.H. Shek, Mater. Sci. Eng. Res 44 (2004) 45.
[40] H.S. Chen, Rep. Prog. Phys. 43 (1980) 353.
[41] M. Stoica, J. Das, J. Bednarcik, G. Wang, G. Vaughan, W.H. Wang, JOM 62 (2010) 76.
[42] ASTM E9-89a, standard test methods of compression testing of metallic materials at room temperature, Annual Book of ASTM Standards, American Society for Testing and Materials, Philadelphia, PA, USA, 2000.
[43] E. Chang, T.M. Lee, Biomaterials 23 (2002) 2917.
[44] ASTM-G31–72, Standard practice for laboratory immersion corrosion testing of metals. Annual book of ASTM standards, American Society for Testing and Materials, Philadephia, Pennsylvania, USA, 2004.
[45] ASTM-G102-89, Standard practice for calculation for corrosion rates and related information from electrochemical measurements, Annual Book of ASTM Standards, American Society for Testing and Materials, Philadelphia, PA, USA, 1999.
[46] ANSI/AAMI, ISO 10993–5, Biological evaluation of medical devices. Part 5. Tests for cytotoxicity: in vitro methods, ANSI/AAMI, Arlington, VA, 1999.
[47] W.H. Wang, J. Appl. Phys. 99 (2006) 093506.
[48] G. Baril, N. Pebere, Corros. Sci. 43 (2001) 471.
[49] S.N. Nomura, K. Oya, Y. Tanaka, R. Kondo, H. Doi, Y. Tsutsumi, Acta Biomater. 6 (2010) 1033.
[50] J.F. Schenck, Med. Phys. 23 (1996) 815.
[51] X.N. Gu, Y.F. Zheng, L.J. Chen, Biomed. Mater. 4 (2009) 056011.
[52] D.R. Lide, CRC handbook of chemistry and physics, 90th Edition CRC press, Boca Raton, FL, 2009.
[53] M. Pourbaix, Atlas of Electrochemical Equilibria in Aqueous Solutions, Pergamon Press, New York, 1966.
[54] F. Feyerabend, J. Fischer, J. Holtz, F. Witte, R. Willumeit, H. Drucker, Acta Biomater. 6 (2010) 1834.
[55] J.R. Popp, B.J. Love, A.S. Goldstein, J. Biomed. Mater. Res. A 81A (2007) 766.
[56] W. Paul, C.P. Sharma, J. Mater. Sci. Mater. Med. 18 (2007) 699.